16th ICAAR LISBOA 2020-2022

16th International Conference on
Alkali-Aggregate Reaction in Concrete
Lisboa | LNEC | Portugal | 31 May - 2 June 2022

http://icaar2020-2022.lnec.pt

Influence of temperature and stress field seasonal variations in the development of concrete swelling in dams. Application to the case of Covão do Meio dam (Portugal)

Ivo Dias [(1)], António Lopes Batista [(2)], Samuel Ferra [(3)]

(1) National Laboratory for Civil Engineering (LNEC), Lisbon, Portugal, idias@lnec.pt

(2) National Laboratory for Civil Engineering (LNEC), Lisbon, Portugal, albatista@lnec.pt

(3) Faculty of Sciences and Technology, New University of Lisbon (FCT/UNL), Portugal, s.ferra@campus.fct.unl.pt

Abstract

This paper presents the study of the influence of temperature and stress field seasonal variations in the development of concrete swelling in dams, considering the case study of Covão do Meio arch dam, in Portugal, which concrete is affected by a moderate ongoing swelling process, of the alkali-silica (ASR) type, and which reservoir empties every year in the dry season.

In a first step, a three-dimensional model of the dam and of the rock mass foundation, solved by the finite element method, was used for the interpretation of the dam's behaviour over time. All relevant actions on the structure were considered, namely the dead weight of the materials, the hydrostatic pressure on the upstream face, the temperature changes in the dam's body and the concrete expansions of internal origin. The structural model considered the concrete viscoelastic behaviour and the influence of temperature and stress fields in the expansion development. The results of the dam's monitoring, of the concrete laboratory tests for diagnosis and prognosis of the concrete properties and of the visual inspections were considered. The monitoring and the numerical results showed an excellent agreement until 2020, attesting the adequacy of the models to simulate the dam's behaviour.

In a second step, the dam's behaviour was simulated considering that the reservoir remains at high levels throughout the year, during all the lifetime of the dam. In this scenario, the computed expansions and its related structural effects decreased of about 10% to 40%, namely in terms of displacements and stresses.

It is concluded, therefore, that the decompression of the dam body and the concrete temperature raise, associated to the reservoir lowering during a significant period of the year, has a great influence on the development of the concrete swelling process and on the related structural effects.

***Keywords**: Concrete swelling (ASR); confinement; temperature variations; finite element method; Covão do Meio dam.*

1 INTRODUCTION

Expansion growth in arch dam's concrete is influenced by the internal temperature and humidity and by the stress state. Seasonal lowering of the reservoirs can increase expansion rates, due to the temperature increase through the upstream face (which is exposed to air temperature and solar radiation) and to the decompression of the dam arches. The goal of this paper is to study the influence of these factors in the free and structural expansions of the concrete, using as a case study the Covão do Meio dam, whose reservoir is empty in summer and full in winter.

The analysis was supported by numerical methods, considering the thermal and structural behaviour of the dam and also the development of the swelling process. In a first stage the models were calibrated and validated, by comparing the monitoring results with the computed values, and then used, in a second stage, to evaluate the influence of the seasonal reservoir lowering in the development of the concrete expansions and in the related structural effects.

2 MODELS AND METHODS

2.1 Structural modelling

The structural modelling is supported by a finite element code, that is at present being development at LNEC, from previous software [1-4]. The analysis is performed incrementally through time, thus the main loads (including the swelling action) are applied according to the selected time discretization.

The concrete delayed behaviour is represented by a linear viscoelastic model, which takes into account the increase of the concrete stiffness over time due to concrete maturing (which is only relevant at early ages), the creep deformations due to applied loads and the stress relaxation due to prescribed deformations (as is the case of the thermal and the expansive actions). Due to computational reasons, the creep function, $J(t, t_0)$ is approximated by a series of real exponentials (Dirichlet series),

$$J(t,t_0) = \frac{1}{E(t_0)} + \sum_{i=1}^{n} \frac{1}{E_i(t_0)} \left(1 - e^{\frac{-(t-t_0)E_i(t_0)}{\eta_i}}\right) \quad (1)$$

which represents the deformation of a Hooke spring and a chain of Kelvin bodies arranged in series (Figure 2.1), where $E_i(t_0)$ are the elasticity modulus depending on time and η_i are the viscosity coefficients.

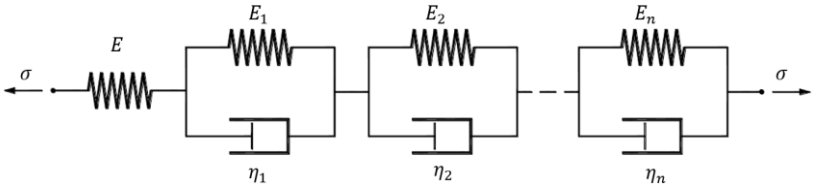

Figure 2.1: Rheological model for the concrete delayed behaviour

The approximation of the creep function through Dirichlet series allows to carry out the structural analysis over time without the need to store the entire load history, so the linear system of equations is solved for all time steps, updating the external loads, the global stiffness matrix and the vectors that store the load history.

Since the expansive process in the dam concrete is of moderate magnitude, it was assumed that the mechanical properties of the concrete are still not effected by internal damages due to swelling. The concrete non-linear behaviour, due to tensile cracking, was also not considered in this study, because structural cracking occurs only in some localized zones of the dam, not affecting its global behaviour.

2.2 Thermal modelling

The temperature distribution across the dam body over time is computed by using a finite element code developed at LNEC [5], that solves the transient heat conduction equation (also known as Fourier's law),

$$k \frac{\partial^2 T(x_i,t)}{\partial x_i^2} + Q(x_i,t) - \rho\, c \frac{\partial T(x_i,t)}{\partial t} = 0 \quad (2)$$

where Q stands for internal heat generation, k for the thermal conductivity, c for the material specific heat, ρ for specific mass, T for the temperature and t for the time.

In this study, the heat generation due to the concrete hydration process is not considered, so the Fourier equation is simplified in the following form, where h^2 is the concrete thermal diffusivity,

$$\frac{\partial T(x_i,t)}{\partial t} - h^2 \frac{\partial T^2(x_i,t)}{\partial x_i^2} = 0 \quad ; \quad h^2 = \frac{k}{\rho\, c} \quad (3)$$

On the external surfaces of the model, both in contact with air and water, heat transfer by convection (Neumann conditions) are considered, according to the following Newton's law of cooling,

$$q = h_c\,(T_w - T_a) \quad (4)$$

where q represents the heat flux normal to the surface, T_w is the surface temperature, T_a is the fluid temperature and h_c is the convection coefficient.

On the surfaces exposed to the air, the effect of solar radiation is also considered through a prescribed heat flux, which depends on the concrete absorption coefficient a and on the incident irradiance I_α,

$$q = a\, I_\alpha \tag{5}$$

The incident irradiance depends on the period of the year, on the time of the day and on the orientation of the exposed surface,

$$I_\alpha = \frac{I_h}{\cos Z}\cos\alpha \tag{6}$$

where I_h is the incident irradiance on a horizontal surface, Z is the angle formed by the vertical line of the location and the line connecting to the sun and α is the angle formed by the incident radiation and the surface normal.

The evolution of the air and water temperatures is represented by sinusoidal waves of annual period, adjusted from the monitoring results,

$$T(t) = T_m + S_a \cos\left(\frac{2\pi}{365}(t-\phi)\right) \tag{7}$$

where T_m is the average annual temperature, S_a is the semi-amplitude and ϕ is the number of days between the beginning of the year and the day of the highest temperature.

2.3 Swelling action modelling

The swelling action is simulated assuming that the structural expansion growth depends on the uncoupled effects of the temperature g_T, the internal humidity g_H and the stress state g_σ, according to the following equation [6],

$$\varepsilon_{exp}(H,T,\sigma,t) = \varepsilon_{exp,\infty}\, \xi_{exp}(t)\, g_H(H)\, g_T(T)\, g_\sigma(\sigma) \tag{8}$$

where $\varepsilon_{exp,\infty}$ is the long-term expansion and ξ_{exp} is a function representing the time evolution of the expansive reaction, varying from 0, for the initial instant of time ($\xi_{exp}(t_0) = 0$), and 1, when the reaction has finished ($\xi_{exp}(t_\infty) = 1$). In this work, for ξ_{exp} is used an exponential sigmoid function, that has a profile similar to the curves obtained in laboratorial tests [7],

$$\xi_{exp}(t) = 1 - e^{-\frac{t^n}{\beta}} \quad ; \quad \beta = \frac{n}{n-1}(t_{hs})^n \tag{9}$$

where t represents time (in days), t_{hs} is the age (in days) corresponding to the curve inflection point and n is a real number that affects the curve shape.

When the exposure cycles to the air of surfaces that are normally submerged are short relatively to the concrete drying process, it can be considered that there is always available water in the dam body to feed the expansive reactions without restrictions (that is $g_H \approx 1$), except in the superficial strips along the faces, during the dry season. This simplification has the advantage to circumvent the need of developing a hygrometric model, for which usually does not exist any observation elements to validate it.

The thermal effect is considered by means of the following expression,

$$g_T(T) = e^{6000\left(\frac{1}{T_{ref}}-\frac{1}{T}\right)} \tag{10}$$

where T_{ref} represents the reference temperature and T is the temperature of the analysed point (in Kelvin).

The structural expansions, that effectively occur in the dam, outcome from restricting the free expansions $\varepsilon_{exp,free}$ by the confining effect of the compressive stresses,

$$\varepsilon_{exp}(H,T,\sigma,t) = \varepsilon_{exp,free}(H,T,t)\, g_\sigma(\sigma) \tag{11}$$

where the factor $g_\sigma(\sigma)$ can be determined from the exponential curve plotted in Figure 2.2, that was adjusted in LNEC to the experimental results obtained by Larive [7] and Clayton [8]. In this study the factor g_σ is considered independently in the three principal stress directions.

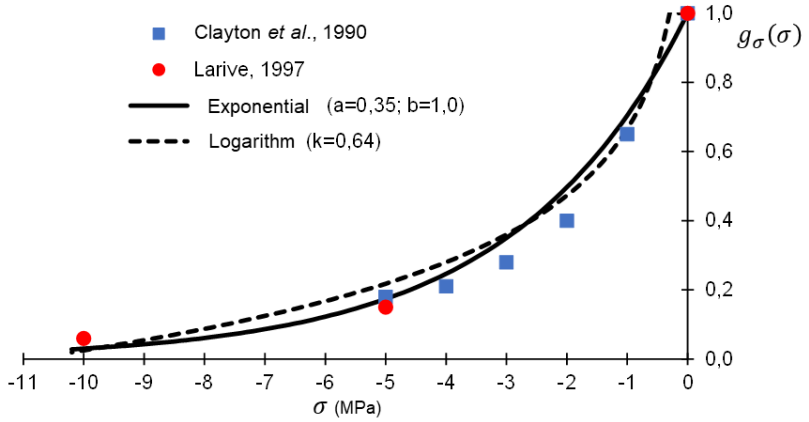

Figure 2.2: Influence of the stress field on the swelling development (taken from [6])

3 CASE STUDY OF COVÃO DO MEIO DAM

3.1 Characteristics of the dam and of its swelling process

3.1.1 Main characteristics of the dam

The Covão do Meio dam, located in the Estrela Mountains at an altitude of about 1650 m, is a thin arch dam, 28 m high, founded on a granite rock mass, with a thickness ranging, in the main cantilever, from 1.8 m at the crest to 6.8 m at the base (Figure 3.1).

Figure 3.1: Covão do Meio dam. View from the right bank in winter

The spillway, located on the left bank, is formed by a gravity structure, 13 m high and 170 m long, that allows to discharge a maximum flow of about 40 m^3/s.

The crest and the retention water level (RWL) are located at levels 1653.90 m and 1653.70 m, respectively (Figure 3.2). For the RWL the reservoir volume is about 1.4 hm^3. The hydrographic basin is only 4.8 km^2.

The dam was built between 1949 and 1953. The concrete was made with coarse granite aggregates and cement contents ranging from 250 kg/m^3 to 300 kg/m^3.

During the winter the water of the reservoir is used for hydroelectric production. During the spring the water is used to irrigate the Loriga agricultural fields. For this reason, the reservoir remains empty, usually, from June to November.

Until 1960, the dam observation was performed by geodetic surveys and visual inspections. After 1960, due to the lower regulation requirements of that period, the dam monitoring was suspended, being resumed in 1981, because of the new safety criteria tendencies. The reference survey for the regular geodetic monitoring was performed in 1985.

The actual monitoring system, that was improved in 1996 and 2000, due to regulation requirements, allows to measure the following physical quantities: i) reservoir level, by a staff gauge and a continuum water level recorder; ii) air temperature, by a PT100 thermometer; iii) concrete temperatures, by embedded resistance thermometers; iv) joint movements, by joint meters and 2D-deformeters; v) water temperatures, by joint meters located on the upstream face (the joint meters allow to measure joint opening/closure movements and also temperatures); vi) horizontal displacements, by plumb lines and geodetic methods; vii) vertical displacements, by precision geometric levelling and by rod extensometers; and viii) discharged and infiltrated flows, by drains and seepage measuring weirs. Due to the adverse weather conditions during the winter and to the site difficult access, some of the installed devices are automatically measured.

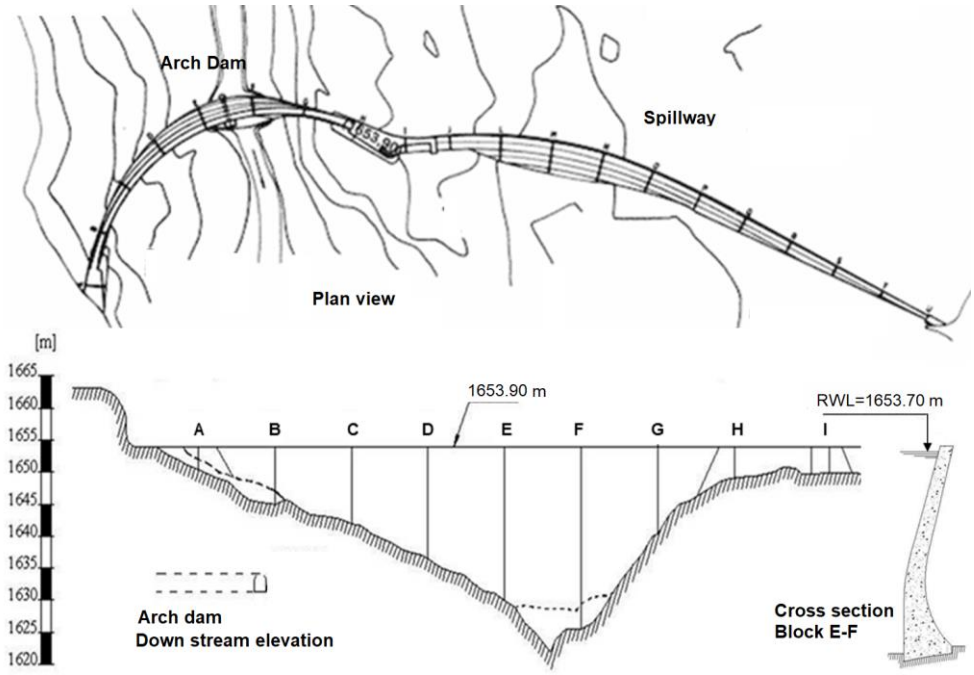

Figure 3.2: Covão do Meio dam. Plan view, downstream elevation and vertical cross-section of the arch

3.1.2 Evidence of the swelling phenomenon and previous studies

The first evidence of the swelling phenomenon was detected in the nineties, about 40 years after the dam construction, being then observed concrete cracking and progressive displacements, vertical upwards and radial upstream. Between 1985 and 2018, the crest of the EF block had upward irreversible displacements of about 18 mm, corresponding to accumulated vertical strains of about 640×10^{-6} in the previous 34 years and to an increase rate of about 32×10^{-6}/year in the previous 5 years. The cracking patterns had progressed considerably since the first mapping performed in 1983 [9], being, at present, observed map cracking on the crest and linear cracking on the downstream face (horizontal in construction joints or parallel to the dam-foundation interface).

In 2005, LNEC developed a study of interpretation of the observed dam behaviour [10], based in a finite element model of the arch dam and the rock mass foundation. The main conclusions drawn from this study were: i) the progressive horizontal and vertical displacements and the joint relative movements are consistent with a swelling process of internal origin; and ii) the linear cracks in the downstream faces are caused by the swelling process, so its evolution should be followed.

Few years later, in 2011, 8 concrete samples were taken from the dam body to characterize, by laboratory tests, the swelling reactions and the mechanical properties of the concrete (modulus of elasticity, compressive and tensile strengths, stiffness damage test, mineralogical analysis, petrographic characterization, cement, sulphate, alkali and silica contents and residual expansion). The tests, that started in 2012 and ended in 2015 [11-12], identified a moderate ongoing swelling process of the alkali-silica (ASR) type. The results of the mechanical tests indicate that the average values of the compressive strength and elasticity modulus of the concrete were about 40 MPa and 25 GPa, respectively. In both cases the results show a high dispersion and depend on the sample location, what can be related to different cement contents used in the dam concrete.

3.2 Finite element mesh, material properties and main actions

3.2.1 Finite element mesh and material properties

A homogeneous continuous model was used since the movements at the contraction joints are very small (the concrete swelling also contributes for closing these joints).

The finite element mesh (Figure 3.3), used for the structural and thermal analyses, has a total of 9336 nodal points for 1848 volumetric 20-node hexahedral finite elements, from which 736 belong to the dam and the remaining 1112 to the rock mass foundation.

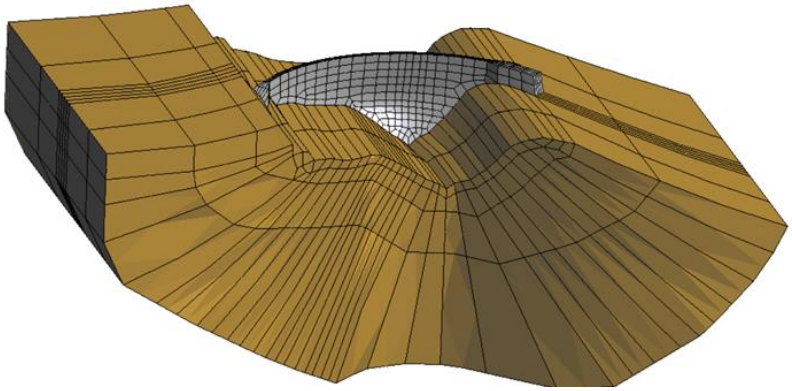

Figure 3.3: Downstream view of the finite element mesh of the arch dam and its rock mass foundation

The rock mass foundation behaviour was considered linear elastic with Young's modulus of 20 GPa and Poisson ratio of 0.2. The deformability of the dam body concrete was simulated by a viscoelastic model, characterized by Poisson ratio of 0.2 and by the Bažant Panula creep law (12), plotted in Figure 3.4 for three ages of loading.

$$J(t,t_0) = \frac{1}{25}(1 + 2.64(t_0^{-0.441} + 0.042)(t - t_0)^{0.168})\ (\mathrm{GPa}^{-1}) \qquad (12)$$

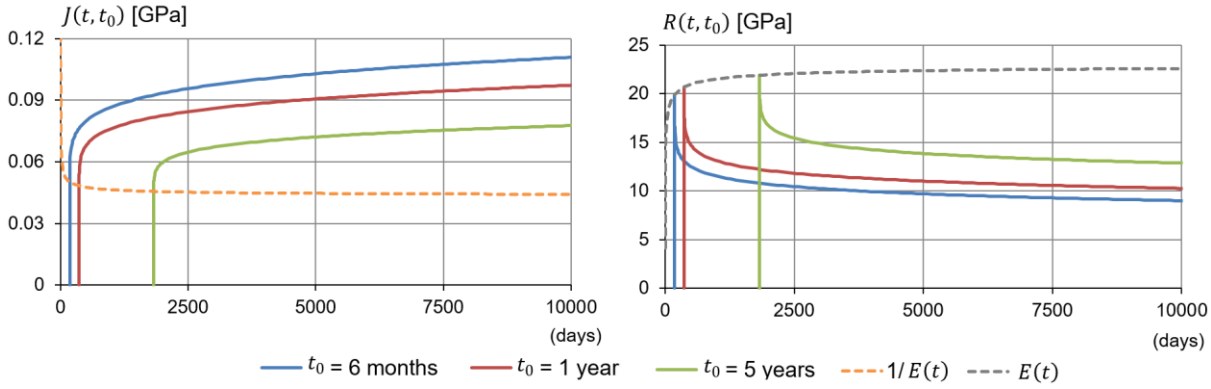

Figure 3.4: Creep $J(t,t_0)$ (on left) and relaxation $R\ (t,t_0)$ (on right) curves of the dam's concrete, plotted for three ages of loading

No specific tests were performed for characterizing the thermal properties of the concrete, being considering the following values, which correspond to average values for the concrete of dams: concrete thermal expansion coefficient $\propto_C = 11 \times 10^{-6}\ /°C$; thermal conductivity $k = 2.6\ W.m^{-1}.K^{-1}$; specific heat capacity $c = 920\ J/(kg.K)$; convection coefficient $h_c = 25\ W.m^{-2}.K^{-1}$; and absorption coefficient $a = 0.65$.

3.2.2 Thermal actions

The thermal wave parameters were determined numerically by the least square method based on the average daily temperatures. For the air, the adjusted wave curve, plotted in Figure 3.5, is characterized by a mean annual temperature of 14.5 ºC and a semi-amplitude of 9.2 ºC. For the water, the temperature variation through depth was considered by 3 curves (Figure 3.6), that were adjusted to the values observed in 3 thermometers, located at different depths on the upstream face.

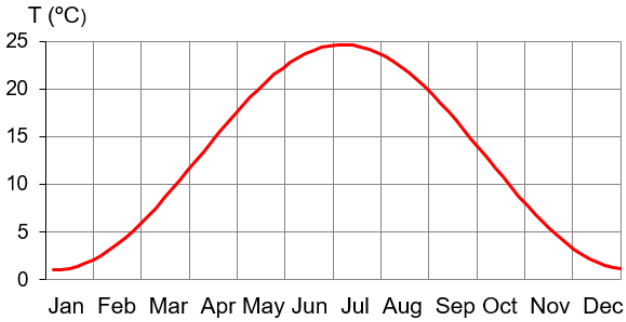

Figure 3.5: Annual thermal wave of the air, evaluated from the monitoring data

Depth (m)	T_m (ºC)	S_a (ºC)	ϕ (days)
1.2	7.96	8.03	208.9
9.4	6.12	4.96	211.56
17.2	4.86	2.88	218.06

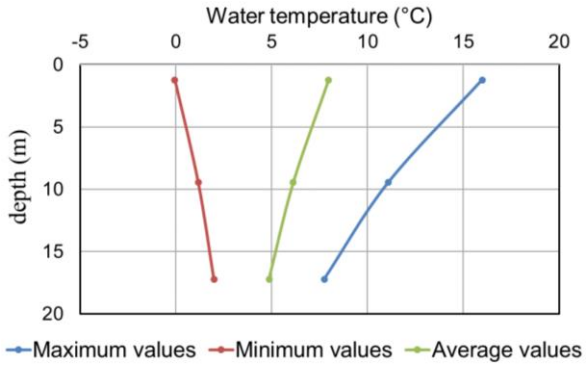

Figure 3.6: Reservoir water. Parameters of the annual thermal wave curve (7) at 3 different depths (left) and variation through depth of the average annual temperature and amplitude (right)

The solar radiation was only considered in the surfaces contacting with the air. For the time domain an hourly discretization was used, which allows to model properly the solar radiation effects.

3.2.3 Swelling action

Figure 3.7 plots the free swelling evolution estimated for a reference temperature of 20º [13].

The dam body was divided in 3 different zones because its vertical displacements, measured by precision levelling, show rather higher deformations on the left bank blocks (see the right plot of Figure 3.12). This zoning is also related with the concrete mix in the different parts of the dam. The estimated free expansions have long-term maximum values ranging from 1200x10^{-6}, in zone A, to 2800 x10^{-6}, in zone C (Table 3.1). The free swelling curves considered the main results of the laboratorial tests [11,12] and were calibrated, over time, by means of an iterative procedure to match the irreversible horizontal and vertical displacements of the dam with the values computed by the model.

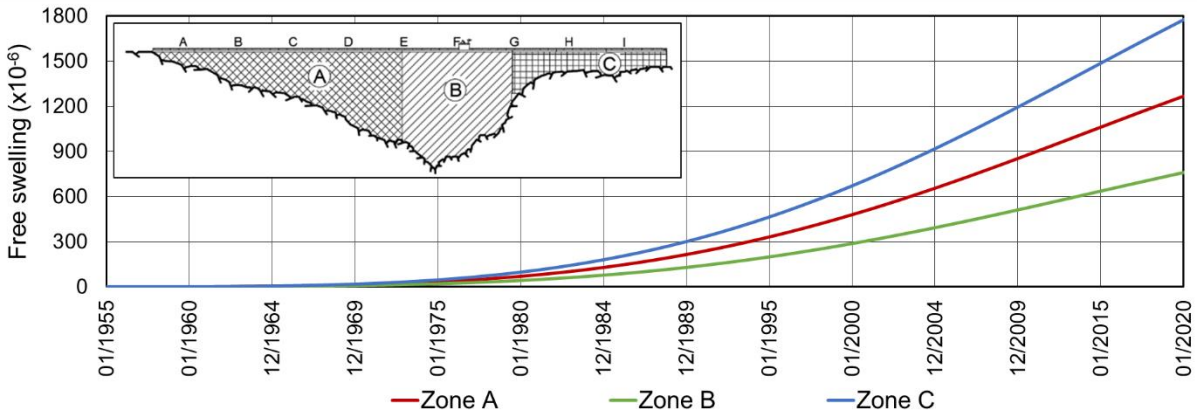

Figure 3.7: Zoning and evolution over time of the free swelling strains in the dam's body for the reference temperature of 20ºC

Table 3.1: Parameters of the curves of the free expansion evolution (3), for the reference temperature of 20ºC

Parameter	Zone A	Zone B	Zone C
n	3.6	3.6	3.6
t_{hs} (days)	22000	22000	22000
ε_∞ (x10^{-6})	1200	2000	2800

The free swelling computed with this action model is heterogeneous along the dam body, since the zones with higher temperatures have more expansions, while the structural expansions are also anisotropic, since the more compressed directions have less expansions.

3.2.4 Structural loads

The main loads acting on the dam, namely the concrete dead weight, the hydrostatic pressure on the upstream face, the concrete temperature variations in the dam's body and the concrete swelling, were applied considering a temporal discretization of two weeks.

The concrete dead weight was applied in the initial stage by means of vertical body forces (γ_c=24 kN/m^3), while the hydrostatic pressure was represented by surface loads (γ_w=10 kN/m^3), according to the reservoir level evolution (Figure 3.8). The concrete temperatures and expansions were computed by using the thermal model and the expansive action model, respectively.

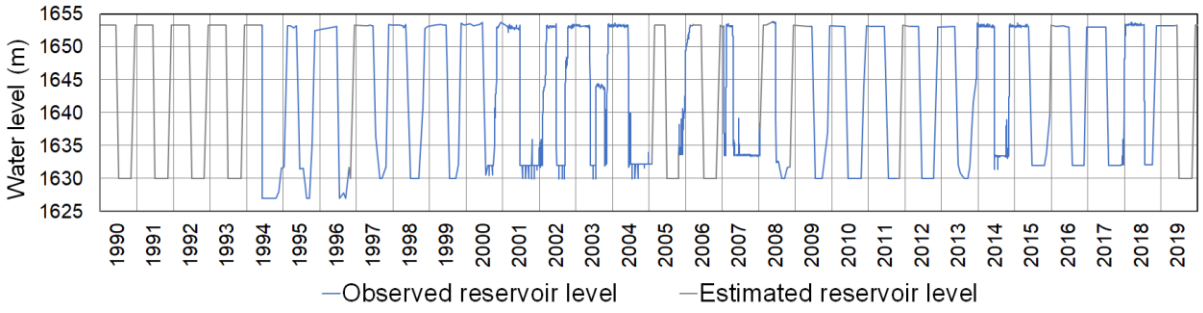

Figure 3.8: Variation of the reservoir water level (the grey segments of the curve correspond to an estimate of the water level in the periods when no monitoring results were available)

3.3 Main results

3.3.1 Interpretation of the dam behaviour for model parameter validation

Figure 3.9 shows the dam thermal field by the 31th December 2019. As expected for this period of the year, the temperatures in the dam body are low (below 5ºC), except in the dam core, near the foundation, where the temperatures are higher (about 10ºC), because of the larger thickness of this section.

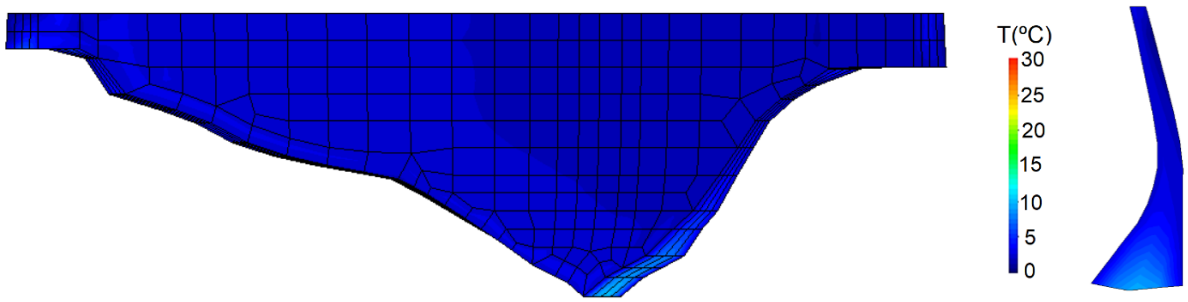

Figure 3.9: Dam thermal field by the 31th December 2019. Downstream face and central cross section

Figure 3.10 illustrates the evolution of the concrete temperatures measured by embedded thermometers and computed by the thermal model, from the beginning of 1998 to the end of 2019. The plots show a reasonable agreement between the computed and the monitoring results.

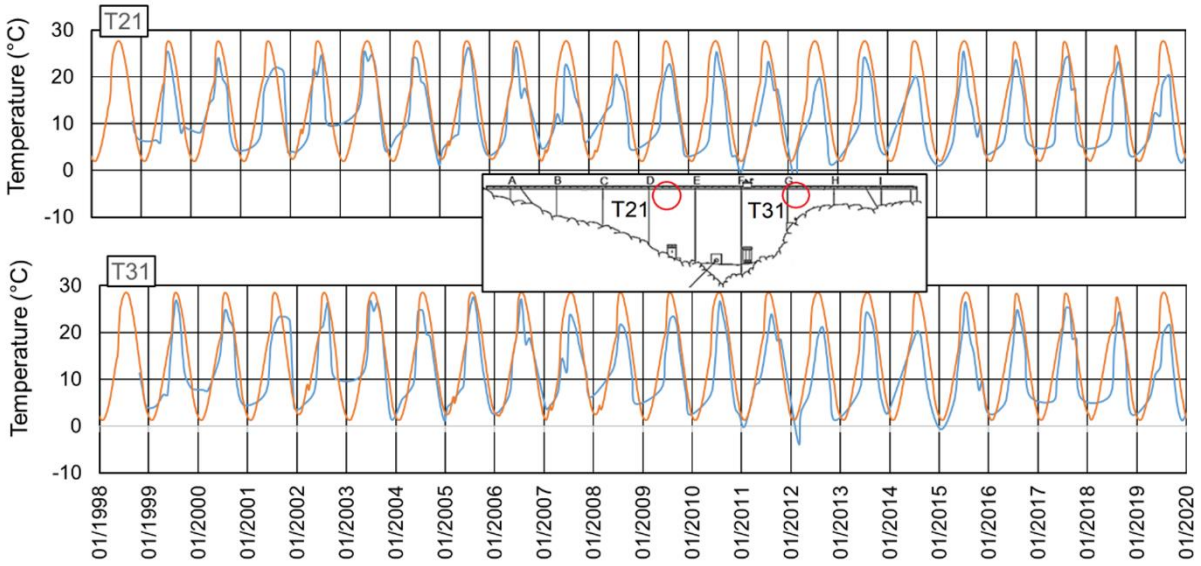

Figure 3.10: Concrete temperatures measured by resistance thermometers and computed with the thermal model

Figure 3.11 shows the evolution of the radial displacements observed by the plumb line 2, at elevation 1653.90 m, and by geodetic methods at a very near mark, from 1985 to the end of 2019, along with the values computed by the numerical model. A good agreement between the computed and the monitoring results is observed. The computed response is also depicted, from the first filling of the reservoir to the end of 2019, in the second plot of the same figure, but there the effects are separately represented, so the relative influence of each effect can be appreciated. It is noticed that after 1970 the dam behaviour ceased to be reversible, being, at present, dominated by the swelling effects (about 30 mm, upstream).

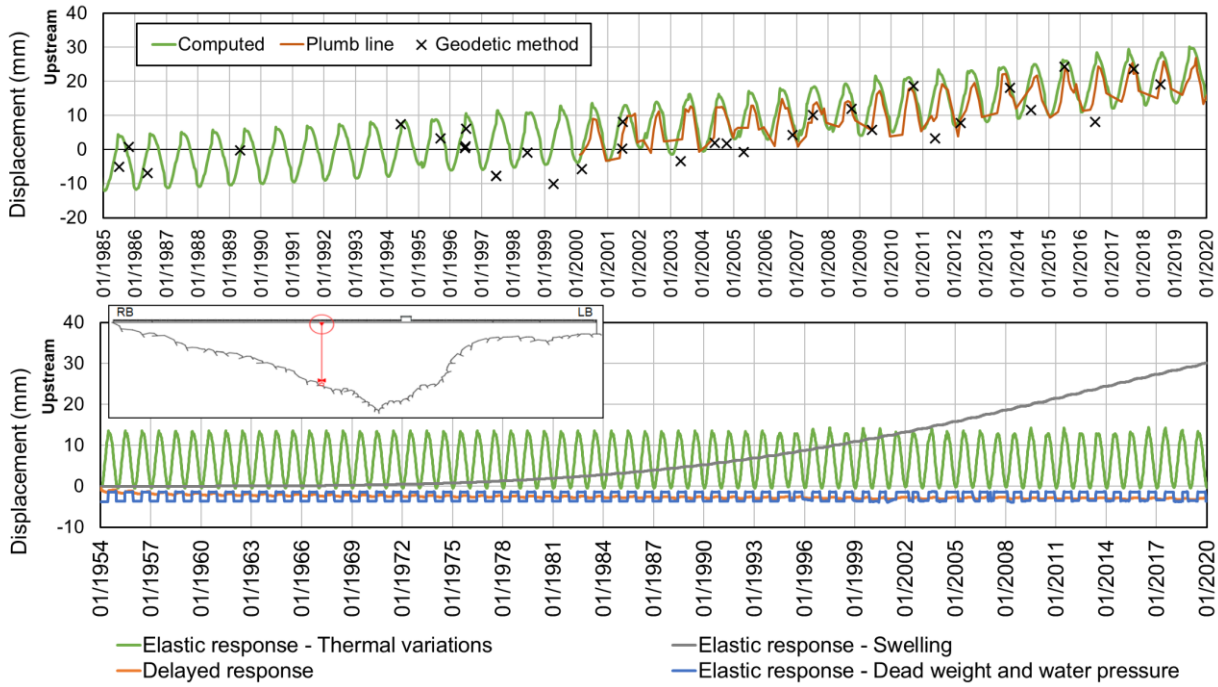

Figure 3.11: Radial displacement measured by the plumb line 2 and by geodetic methods and computed by the structural model

The left plot of Figure 3.12 presents the vertical deformed shape of the crest between 1985 and 2018, observed by precision levelling and computed by the structural model, while the right plot presents, for the same period, the average vertical strains (these values were computed dividing the vertical displacements by the average high of the block). For both cases a very good agreement between the monitoring and the computed results is observed, for all levelling marks. The right plot of Figure 3.12 also evidences that the average expansions in the left bank blocks are much higher that the values of the right bank blocks.

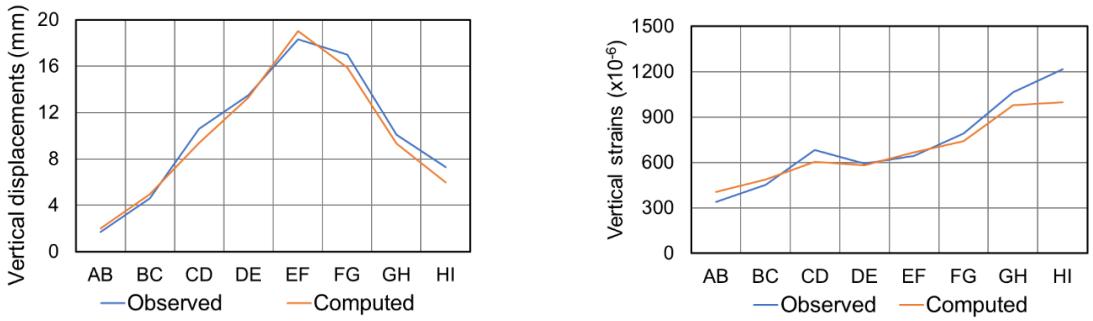

Figure 3.12: Vertical deformed shape of the crest between 1985 and 2018 (left) and average vertical strains of the blocks between 1985 and 2018 (right)

Figure 3.13 presents the principal stresses on the upstream and downstream faces, calculated in the end of 2019, due to the combined loads of the dead weight, hydrostatic pressure, swelling and as well as their delayed effects. The stress field is predominantly compressive. The higher compressive stresses are parallel to the dam-foundation interface, reaching about 9.8 MPa near the left bank bearing, downstream. The maximum tensile stresses occur also on the downstream face of the left bank blocks, but are normal to the dam-foundation interface, with values reaching about 5.6 MPa. On the right side of the dam the maximum tensile stresses reach 3.6 MPa, also near the dam-foundation interface. These high tensile stresses are consistent with the linear cracks observed in localized zones of the downstream face, near the foundation. Since the structural cracks occur only in relatively small zones of the dam, the effect of the cracking on the global structural behaviour is also small, but, locally, some stress redistribution occurs, which is not simulated by the adopted structural model.

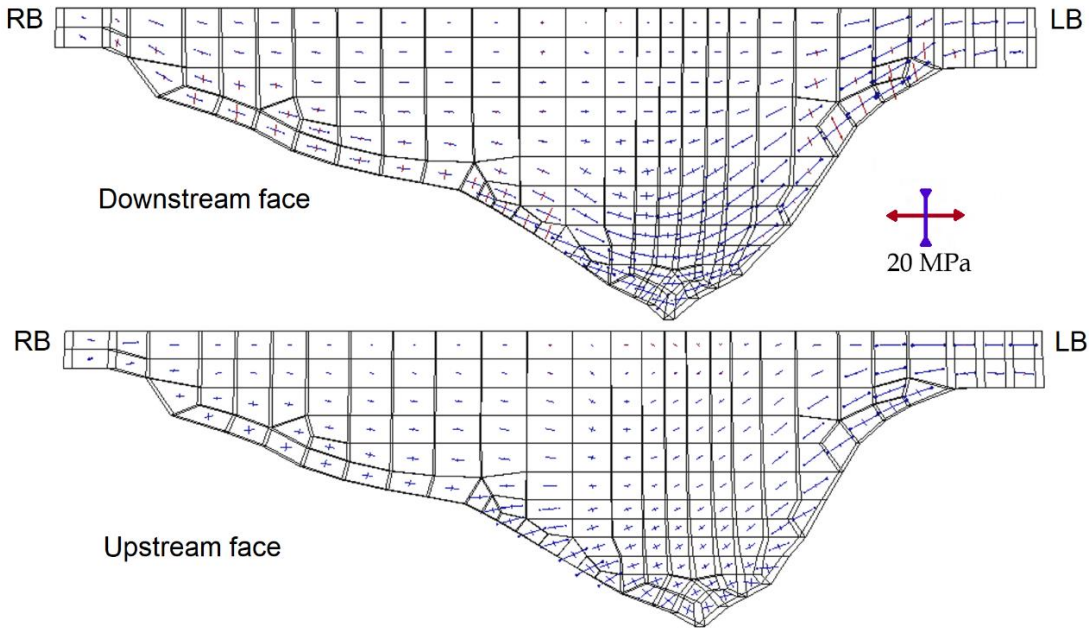

Figure 3.13: Principal stresses on the dam faces computed at the end of 2019, due to the combined loads of the dead weight, hydrostatic pressure and swelling

3.3.2 Influence of temperature and stress field seasonal variations in the structural response

The management of the Covão do Meio reservoir is seasonal, being empty and full in the dry and the wet seasons, respectively. Expansion grow might increase during the periods of empty reservoir, because of the next cumulative reasons:

1) Concrete temperature increase – when the reservoir empties during the dry season, the upstream face is exposed to higher temperatures and to the solar radiation, which increase the free swelling;
2) Confining stresses decrease – the reservoir emptying in the dry season leads to the structural decompression of the arches, which increases the structural expansions in this direction.

To study the influence of these two factors, a second scenario (called scenario B) was considered, where the reservoir remains full, near the RWL (1653.3 m), during all the dam lifetime. For scenario B, all models (thermal, structural and expansive action) were updated and new calculations were made.

Moreover, to separate the influence of the confining stresses from the influence of the temperature variations, a third scenario was considered (scenario C), where the reservoir remains also full, but the temperature variations and free swellings of scenario A were applied (for this case only the structural model needed to be updated). Since scenarios A and C have the same free swelling, the influence of the confining stresses can be straightforward evaluated.

Figure 3.14 shows, on the left side, the temperature distribution on the highest cross section of the dam for the scenarios A and B. It is observed that temperatures in the upper part of the cross section for scenario A are rather high and constant through the thickness, while for the scenario B there is a downstream-upstream gradient, with a hot downstream face and much cooler upstream face. The temperature evolution at point T during 2019, plotted on the right side of Figure 3.14, shows that the differences between scenarios arise when the reservoir empties (in the mid-June), being higher in mid-July, when the temperature variation for scenario A is about 10ºC higher than for scenario B.

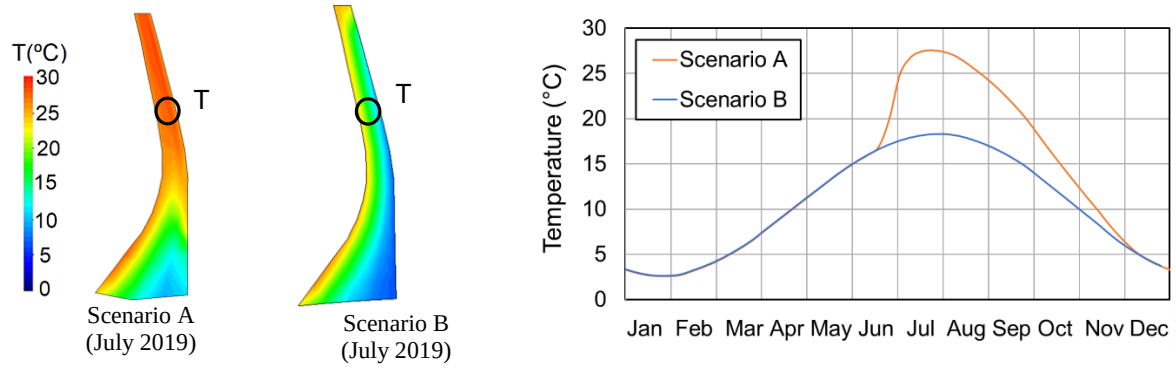

Figure 3.14: Thermal fields for scenarios A and B in the highest dam cross section (left). Temperature evolution at the point T, at 1643.90 m elevation, during 2019

Figure 3.15 depicts the free swelling evolution, since the first filling of the reservoir until the end of 2019 and also during 2019, at points at elevation 1651.0 m of the joint E (upstream and downstream), for the scenarios A and B. At the downstream face the free swellings are very similar for both scenarios, while at the upstream face the expansions are about 25% smaller for the scenario B (due to the lower temperature of the face for this scenario).

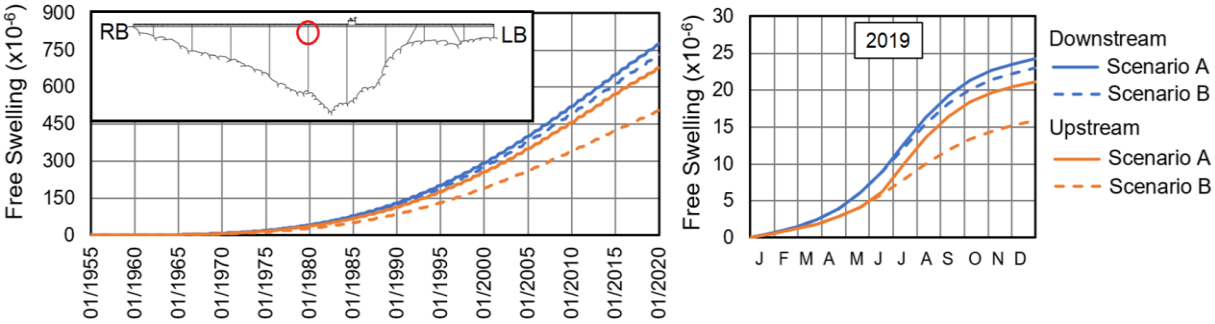

Figure 3.15: Free swelling evolution at the point at elevation 1651.0 m of joint E (upstream and downstream), for scenarios A and B, from the first filling of the reservoir to the end of 2019 (on the left) and during 2019 (on the right)

Figure 3.16 presents the evolution of the structural expansions at a point of joint E, at elevation 1651.0 m, on the upstream face, for scenarios A and C. The expansions on the arch direction ($\varepsilon_{exp,arc}$) are smaller for scenario C, because the compressive stresses, due to the permanent hydrostatic load, constrain the growth of the structural expansions in this direction. On the other hand, since no relevant vertical compressions occur at this point due to the hydrostatic pressure, the vertical expansions curves ($\varepsilon_{exp,ver}$) are very close for both scenarios.

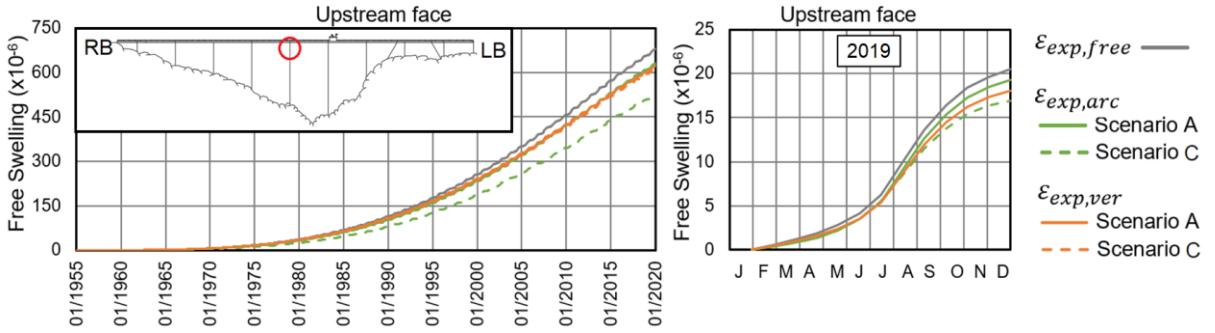

Figure 3.16: Structural expansions evolution (arch and vertical directions) at a point of joint E, at elevation 1651.0 m, upstream, for scenarios A and C, from the first filling of the reservoir to the end 2019 and during 2019

Tables 3.2 and 3.3 summarize the results obtained for the different scenarios, at points corresponding to the monitoring devices installed in the dam. The displacements are until 38% higher in scenario A relatively to scenario B. For the vertical displacements, the differences are mainly due to the effect of

the concrete temperature (10% to 15%) and, in a much lower degree, due to the stress confining effect (less than 3%), because vertical compressive stresses, associated to the hydrostatic pressure, are circumscribed to the zones of the downstream face near the rock mass foundation. On the other hand, the differences found on the radial displacements are both due to the influence of confinement (less than 22%) and of temperature (less than 17%).

Table 3.2: Vertical displacements at points corresponding to the levelling marks for the different scenarios and influence of the confining stresses and of the concrete temperature

	Scenario A	Scenario C	Scenario B	Effect of the confinement decrease (A – C)		Effect of the temperature increase (C – B)		Effect of the confinement and temperature (A – B)	
	mm	mm	mm	mm	%	mm	%	mm	%
AB	2.8	2.8	2.5	0.0	0.0	0.3	12.3	0.3	11.7
BC	6.6	6.6	6.0	0.0	0.0	0.6	9.7	0.6	9.6
CD	12.1	12.0	10.8	0.2	1.4	1.2	9.7	1.3	11.1
DE	16.9	16.4	14.6	0.5	2.9	1.8	10.9	2.3	13.8
EF	24.1	23.4	20.3	0.6	2.7	3.2	13.1	3.8	15.8
FG	19.9	19.8	17.4	0.1	0.7	2.4	12.1	2.6	12.8
GH	11.7	11.8	10.3	-0.1	-0.9	1.5	13.1	1.4	12.1
HI	7.7	7.7	6.5	0.0	0.1	1.2	15.3	1.2	15.4

Table 3.3: Radial displacements at points corresponding to plumb lines bases and geodetic marks for the different scenarios and influence of the confining stresses and of the concrete temperature

	Scenario A	Scenario C	Scenario B	Effect of the confinement decrease (A – C)		Effect of the temperature increase (C – B)		Effect of the confinement and temperature (A – B)	
	mm	mm	mm	mm	%	mm	%	mm	%
FPI1	46.1	40.4	38.4	5.7	12.4	2.0	4.3	7.7	16.6
FPD2	30.1	26.7	26.0	3.3	11.1	0.7	2.4	4.1	13.5
CD53B	27.5	26.3	25.5	1.2	4.3	0.8	3.0	2.0	7.3
CD43B	8.1	7.3	6.4	0.8	9.8	0.9	11.4	1.7	21.1
DE53B	30.7	27.6	26.7	3.1	10.1	0.9	2.9	4.0	13.0
DE43B	14.7	12.0	10.3	2.7	18.4	1.7	11.6	4.4	30.0
EF53B	45.0	38.4	36.3	6.6	15.2	2.0	4.5	8.6	19.6
EF43B	25.5	20.1	15.8	5.4	21.6	4.3	16.9	9.7	38.1
FG53B	42.9	39.2	38.0	3.8	9.5	1.1	2.6	4.9	11.4
FG43B	14.3	11.8	9.2	2.4	17.9	2.5	17.9	5.0	35.1

4 CONCLUSIONS

The mathematical methodologies used in this study to interpret the behaviour of the Covão do Meio dam, were adequate for its propose since the monitoring and the numerical results showed an excellent agreement. These methodologies were also used to study the influence of the concrete seasonal variations of temperature and stress on the development of the concrete swelling.

The impact of the dam decompression and of the concrete temperature raise, associated to the reservoir lowering during a significant period of the year, in the evolution on the free and structural expansions was found to be significant. The free swellings increase substantially near the upstream face (due to the higher temperature of this face), while the structural expansions increase considerably on the zones where the constrain of the free swellings depends mainly on the compressions due to the hydrostatic pressure.

The dam displacements are up to 38% higher than what could occur if the reservoir was explored close to the RWL:

1) The average increase of the vertical displacements at the crest was essentially due to the temperature effect (about 12%), what was expected since the hydrostatic pressure only originate vertical compressions in the downstream face near the rock mass foundation;
2) The average increase of the radial displacements is influenced by the arch decompression (about 10% at the crest and about 17% at 1643.0 m elevation), and, in a lower degree, by the temperature (about 3% at the crest and about 14% at 1643.0 m elevation).

ACKNOWLEDGMENT

Thanks are due to EDP, owner of Covão do Meio dam, for permission to present the dam monitoring results.

REFERENCES

[1] Batista A (1998) Analysis of the behaviour over time of arch dams (in Portuguese). PhD thesis, Instituto Superior Técnico, Lisbon.

[2] Oliveira, S (2000) Models for analysing the behaviour of concrete dams considering cracking and the time effects. Damage formulation *(in Portuguese)*. PhD thesis, Faculdade de Engenharia da Universidade do Porto, Porto.

[3] Piteira Gomes J (2007) Structural behaviour modelling of concrete dams subject to swelling reactions *(in Portuguese)*. PhD thesis, Faculdade de Ciências e Tecnologia, Universidade Nova de Lisboa, Lisbon.

[4] Dias IF, Oliver J, Huespe AE (2012) Strain injection techniques in numerical modeling of propagating material failure. Monograph CIMNE M134. International Center for Numerical Methods in Engineering, Barcelona.

[5] LNEC (Leitão N) (2012) Thermal analysis of concrete dams: Environmental thermal actions *(in Portuguese)*. Report 185/2012, DBB/NMMF, Lisbon.

[6] Batista A (2021) Structural management and rehabilitation of dams affected by concrete swelling reactions *(in Portuguese)*. Research program, LNEC, Lisbon.

[7] Clayton N, Currie RJ, Moss RM (1990) The effects of alkali-silica reaction on the strength of prestressed concrete beams. The Structural Engineer, 68, N. 15, p. 287-292.

[8] Larive C (1997) Apports combinés de l'expérimentation à la compréhension de l'alcali-réaction et de ses effets mécaniques. PhD thesis, École Nationale des Ponts et Chaussées, Paris, France.

[9] LNEC (Matos M) (1986) Monitoring of the Covão do Meio dam. Mapping of the cracks on the downstream and upstream faces *(in Portuguese)*. Report 156/1986, DB/NO, Lisbon.

[10] LNEC (Oliveira S, Mendes L, Dias IF, Ramos J) (2006) Covão do Meio dam. Behaviour analysis and assessment of the safety conditions *(in Portuguese)*. Report 58/2006, DBB/NMMF/NO, Lisbon.

[11] LNEC (Santos Silva A, Custódio J, Costa D) (2013) Covão do Meio dam. Assessment of the state of degradation of concrete based on the results of laboratory tests carried out in 2012 *(in Portuguese)*. Report 62/2013, DM/NMM/NPC, Lisbon.

[12] LNEC (Custódio J, Santos Silva A, Costa D) (2015) Covão do Meio dam. Assessment of the state of degradation of the concrete based on the results of laboratory tests. Final Report *(in Portuguese)*. Report 310/2015, DM/NBPC, Lisbon.

[13] Ferra, S (2022) Study of the influence of large seasonal temperature and stress variations on the development of concrete swelling in dams *(in Portuguese)*. Master thesis, Faculdade de Ciências e Tecnologia, Universidade Nova de Lisboa, Lisbon.